

Simple Book Example

TeXstudio Team

January 2013

ii

thesis

Contents

1	Simulation of a plenoptic 2.0 system	3
1.1	Rendering in Plenoptic 2.0	4
1.1.1	Extracting sub images	6
1.1.2	Basic Rendering	7
1.1.3	Depth based rendering	9
1.2	Description of the system	12
1.3	Optical performances of a focused plenoptic system	17
1.4	Impulse response of a Focused Plenoptic system	21
1.5	Two point resolution	25
1.6	Frequency analysis of a focused plenoptic system	28
1.7	Conclusions	42
2	Conclusions and Future work	45

List of Figures

1.1	Top: the point A is imaged by the main lens into the point a' . A' is imaged by the lens let array into a number of sub imaged depending by the magnification of the micro array stage, in this case $m=0.333$. Bottom: particular of the raw image af the point source A and phase space diagram. The three sub images 1,2, and 3 are three different points of view of the object.	5
1.2	Relation between the position of the centre of a lens let x and the position of the centre of the correspondent sub image $x + x'$	7
1.3	Basic rendering algorithm. The Rendered image is composed tiling together patches extracted by each sub image. The patch size is dependent by the magnification of the micro array stage.	8
1.4	The points that belongs to the object plane represente in red are imaged on a virtual main lens image plane. This plane is relayed on a virtual sensor plane by a virtual micor array whose parameters are a' and b' and $m' = b'/a'$	10
1.5	11
1.6	Ray diagram of the system simulated.	12
1.7	Values of the parameter b correspondent to values of magnification varying from 0.1 to 0.5.	14
1.8	Values of the parameter b correspondent to values of magnification varying from 0.1 to 0.5.	15
1.9	Aperture of the main lens as a function of the magnification in order to respect the f-number matching condition.	16
1.10	Aperture of the main lens as a function of the magnification in order to respect the f-number matching condition.	18
1.11	lateral resolution as a function of the magnification.	20
1.12	optical cut-off frequency as a function of the magnification.	20
1.13	Left: raw sensor image, Right: rendered image. Artifacts are present. Magnification: 0.5	22

1.14 Left: raw sensor image, Right: rendered image. Artifacts are present. Magnification: 0.3.	22
1.15 Left: raw sensor image, Right: rendered image. Artefacts are present. Magnification: 0.25	23
1.16 From top to bottom: comparison between the main lens image profile, in blue, and the rendered image profile, in red, for magnification values of 0.5,0.3 and 0.25. The central lobe of the rendered image increase with the magnification, as well as the number of artefacts.	24
1.17 On the top left it is shown the main lens image of two point sources separated by the Rayleigh distance δx . On the top right its corresponded rendered plenoptic image obtained with a magnification of 0.5. As expected from the theory, the resolution of the rendered image is half the one of the main lens image, and the two points are no more distinguishable as confirmed by the intensity profiles of the two images on the bottom.	26
1.18 In the top left it is shown the main lens image of two point sources separated by the Rayleigh distance $2\delta x$. On the top right its corresponded rendered plenoptic image obtained with a magnification of 0.5. Doubling the Rayleigh distance we obtained a rendered image at the limit of resolution, where the maximum of the Airy pattern of one point falls on the first zero of the second point.	27
1.19 Modulation transfer functions of the main lens (green) and the overall imaging system (red) for a magnification value of $m = 0.5$	29
1.20 Modulation transfer functions of the main lens (green) and the overall imaging system (red) for a magnification value of $m = 0.3$	30
1.21 Modulation transfer functions of the main lens (green) and the overall imaging system (red) for a magnification value of $m = 0.25$	30
1.22 The object imaged in this simulation is a sinusoidal grating containing five different frequencies.	32
1.23 Top: on the left it is shown the raw sensor image, on the right the main lens image. Bottom: On the left there is the rendered image, on the right the same image has been low pass filtered to remove some of the rendering artefacts. Magnification was 0.5	33

1.24 On the left are plotted the intensity profiles of the main lens image, top and of the rendered image, bottom. Spatial frequencies are modulated according to the MTF as shown by the power spectra of the main lens image on the top right and of the rendered image on the bottom right. The magnification of the lens let array is $m = 0,5$ and cut-off frequency of the system is $f_{cut-off} = 10^{41}/m$	34
1.25 Evolution of the spectrum of the optical field as it propagates through the imaging system. The imaging system is modelled as a linear low pass filter with a bandwidth δf_2 defined by the magnification of the micro array stage.	35
1.26 Top: on the left it is shown the raw sensor image, on the right the main lens image. Bottom: On the left there is the rendered image, on the right the same image has been low pass filtered to remove some of the rendering artefacts. Magnification was 0.3.	37
1.27 On the left are plotted the intensity profiles of the main lens image, top and of the rendered image, bottom. Spatial frequencies are modulated according to the MTF as shown by the power spectra of the main lens image on the top right and of the rendered image on the bottom right. The cut-off frequency of the system is $0.756 \times 10^{41}/m$	38
1.28 Aliased frequencies transmitted to the rendered image.	39
1.29 Top: on the left it is shown the raw sensor image, on the right the main lens image. Bottom: On the left there is the rendered image, on the right the same image has been low pass filtered to remove some of the rendering artefacts. Magnification was 0.3.	40
1.30 On the left are plotted the intensity profiles of the main lens image, top and of the rendered image, bottom. Spatial frequencies are modulated according to the MTF as shown by the power spectra of the main lens image on the top right and of the rendered image on the bottom right. The cut-off frequency of the system is $0.6 \times 10^{41}/m$	41

Intruduction

Chapter 1

Simulation of a plenoptic 2.0 system

In this chapter several simulation works performed to characterize the optical performances of a focused plenoptic imaging system will be presented. The scope of this work is to investigate the behaviour of a plenoptic 2.0 imaging system at its diffraction limit under a wave optics approach. All simulations described in this chapter have been run using the home made Fresnel Simulation Toolbox described in chapter ???. In a plenoptic 1.0 imaging system the resolution is limited by the dimensions of lens lets [25] and the final rendered image suffers has a much lower resolution then a conventional image. In a focused plenoptic system, as explained in section ???, the resolution of the final rendered image is not linked any more to the number of lens let in the micro array and it is possible to recover the full sensor resolution pushing it even to sub-pixel resolution. [11, 12, 26]. This characteristic makes plenoptic systems suitable to a wider range of applications where high spatial resolution is required [27]. In the past years further effort has been made to push plenoptic 2.0 system to achieve super-resolution performances [28, 26, 29].

However it is limited sub pixel resolution and the term super-resolution is not referred to the achievement of a resolution beyond diffraction limit[30] but to a digital resolution only. Especially when applied to microscopy diffraction still represents a big limitation for plenoptic imaging systems. In this chapter will be shown how diffraction affects the optical resolution of the imaging system and how it is linked to the spatio-angular trade off [31]. Numerical simulations will be used implemented by the platform described in chapter ??.

1.1 Rendering in Plenoptic 2.0

As introduced in chapter ??, rendering an image from a plenoptic 2.0 raw data is based on integrating for each position all the correspondent directional coordinates. While in plenoptic 1.0 each position is sampled by a single lens let, that causes the loss of resolution in the final image, in plenoptic 2.0 each position is sampled by several lens lets. Therefore with reference to figure 1.1, the spatial coordinate (x,y) of point A will be sampled by the lens lets 1,2 and 3, therefore A is represented by 3 sub images. Each sub image is a different point of view of A and directional coordinates are sampled by these three point of view simultaneously. The number of sub images into which the point *A* is imaged depends by the magnification $m=b/a$ of the lens let array and is given by:

$$N_{sub} = \frac{1}{m} = \frac{a}{b} \quad (1.1)$$

a is the distance of the micro array from the main lens image and *b* is the distance of the from the sensor plane.

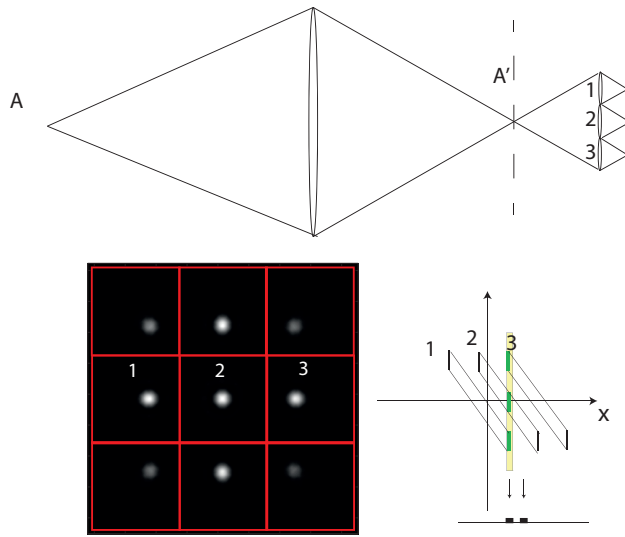


Figure 1.1: Top: the point A is imaged by the main lens into the point a' . A' is imaged by the lens let array into a number of sub imaged depending by the magnification of the micro array stage, in this case $m=0.333$. Bottom: particular of the raw image af the point source A and phase space diagram. The three sub images *1,2, and 3* are three different points of view of the object.

From a computational point of view the basic rendering is performed directly on the raw sensor image and has following steps:

- the single sub images are isolated one from the others
- according to the magnification m we define the number of angular samples to be extracted by each sub image.
- the number of pixel corresponding the number of samples to extract are extracted by the sub image and tiled all together forming the rendered image.

1.1.1 Extracting sub images

Isolating the sub image is an apparent simple task that must be done with extreme care in order to preserve the integrity of the sub images correcting the radial distortion due to geometrical optics caused by the main lens. The radial distortion, also known as pincushion effect, consist in an uniform magnification increase with the increasing of the distances form the centre of the image [24]. Hence the effects of this distortion are more sensitive on the sub images on the edges of the raw data that are misaligned respect the regular square grid of the micro lens array. With reference to figure 1.2 we have:

$$\frac{x}{z+a} = \frac{x'}{b} \quad (1.2)$$

Therefore each lenslet is shifted of a quantity:

$$x' = \frac{xb}{z+a} \quad (1.3)$$

Since $z \approx z + a$ we have that the centres of each sub image are shifted of a quantity equal to:

$$x' = x \frac{b}{z} \quad (1.4)$$

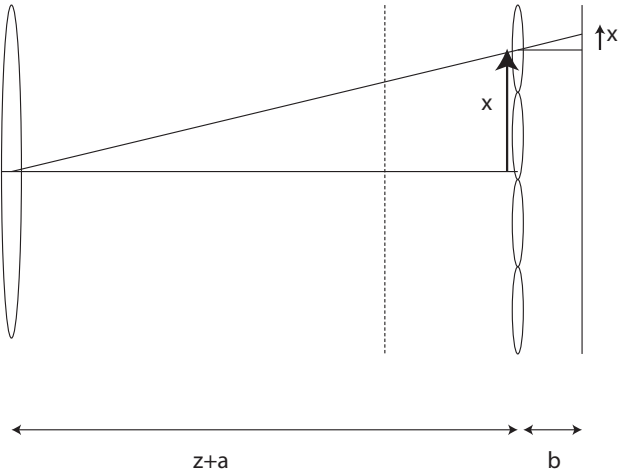


Figure 1.2: Relation between the position of the centre of a lens let x and the position of the centre of the correspondent sub image $x + x'$.

In figure 1.2 x is the position of the centre of a micro lens and its correspondent sub image will be shifted of a quantity x' . The distortion x' increases with the increasing of the distance from the centre and depends by the distance of the image plane from the main lens z and the distance of the sensor form the micro lens b . Once localized the centres of the sub images it is possible to extract each one of them from the raw data and perform the rendering.

1.1.2 Basic Rendering

In this section will be shown how it works the basic rendering algorithm analysed from a theoretical point of view in section ?? as described by Georgiev and Lumsdaine *et al.* [3, 12]. The raw image on the sensor plane is a relay of the main lens image plane [3]. Each sub image represents a single point of view of an area of the main lens image plane. Referring to figure 1.3, if the micro array is composed by N by N lens lets, the raw sensor image

will be composed by an N by N array of sub-images. Each sub-image has a dimension of P by P where P is the micro lens pitch.

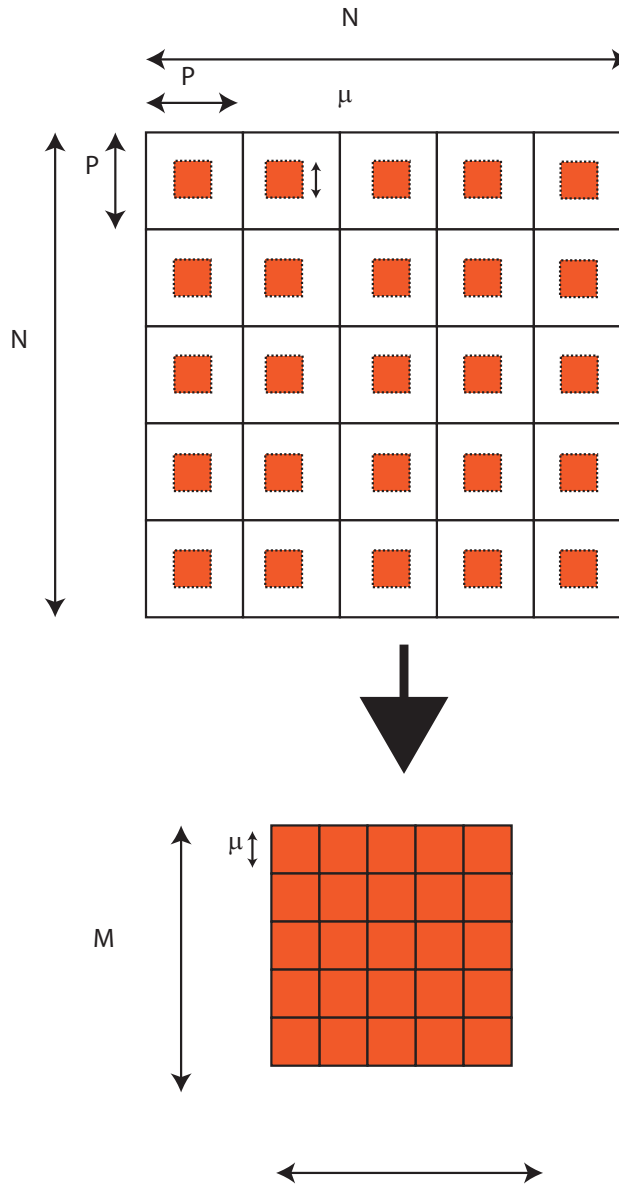


Figure 1.3: Basic rendering algorithm. The Rendered image is composed tiling together patches extracted by each sub image. The patch size is dependent by the magnification of the micro array stage.

The magnification of the micro array is $m=b/a$ and each micro lens maps

the main lens image on the sensor plane on a sub image magnified of a quantity m . Therefore from each sub image we select a patch with a dimension equal to:

$$\mu = P \frac{b}{a} = Pm \quad (1.5)$$

The patch size depends on the magnification of the lens lets array. In the next section will be shown how this fact can be used to recover depth information from the raw sensor images.

1.1.3 Depth based rendering

The patch size μ as seen in equation 1.5 depends by the magnification of the micro array stage. If the point imaged is out of focus, its image will be formed on a different plane than in not the main lens image plane. Hence the main lens image will be blurred and so will be the sub images on the sensor. If during the rendering process we take into account that a point at a different depth respect the main lens focal plane will be imaged at a different distance from the micro lens array, it is possible to define a new value of magnification m' to which will correspond a new patch size μ' . With reference to figure 1.4, the points that belongs to the plane showed represented by the dashed red line placed at a distance d from the object plane, will be imaged on a plane in between the main lens and the main lens image plane. It is possible to define a virtual micro array stage respect this plane for which its points will be imaged in focused on a virtual sensor plane. The parameters characterizing the virtual micro array stage are the distances a' and b' and a magnification $m' = b'/a'$.

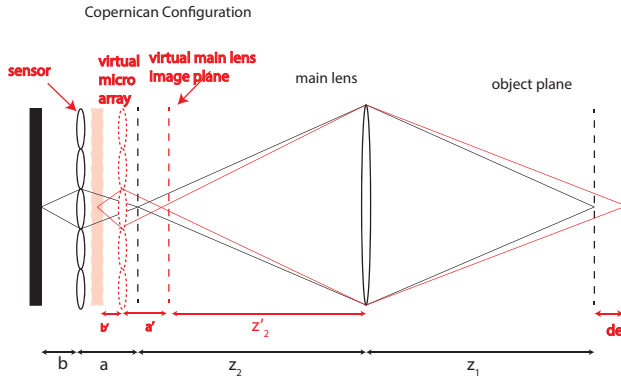


Figure 1.4: The points that belongs to the object plane represente in red are imaged on a virtual main lens image plane. This plane is relayed on a virtual sensor plane by a virtual micor array whose parameters are a' and b' and $m' = b'/a'$.

The distance between the main lens image plane and the virtual main lens image plane, defined as $\alpha = a - a'$, is called virtual depth [32]. It is linked to the actual defocus of the object plane by the lens law referred to the main lens. The magnification of the virtual lens let array defines the patch size to use to rendered the point at that particular depth. The link between the magnification m' and m can be defined applying two time the lens law, one time for the main lens and on for the micro array stage. We have that the virtual main lens plane corresponding to a defocus d is:

$$z'_2 = \frac{(z_1 + d)f}{(z_1 + d) + f} \quad (1.6)$$

f is the focal length of tha main lens. The corresponding virtual depth value is given subtracting the quantities z'_2 and z_2

$$\alpha = z'_2 - z_2 \quad (1.7)$$

Then from the virtual depth α we can obtian the values a' and b' for the

virtual micro array.

$$\begin{cases} a' = a - \alpha \\ b' = \frac{a'f}{a' + f} \end{cases} \quad (1.8)$$

And the magnification for the virtual plane is:

$$m' = \frac{b'}{a'} \quad (1.9)$$

Values of the magnification m' plotted in function of the defocus are shown in figure 1.5

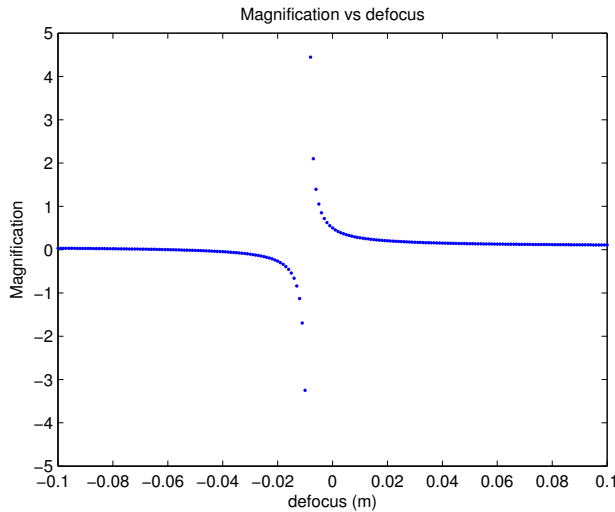


Figure 1.5: .

The patch corresponding to the new focal plane is therefore:

$$\mu' = Pm' = P \frac{b'}{a'} \quad (1.10)$$

Rendering with the new patch size allows to refocus at a different plane. If the defocus is not known, as it happens in the majority of the cases, is it possible to estimate the depth information of the scene imaged and using this information to render the final image. This algorithms are based on cross

correlating each sub images with its close neighbours in order to evaluate the relative shift due to a change in depth across the lens let[33, 34]. In this way it is possible to determine the patch size that results in the best match with all of its neighbours [3, 11]. The axial resolution of a plenoptic 2.0 system is determined considering that the minimum shift between neighbours lens let is the one equal to one pixel.

1.2 Description of the system

The system simulated is shown in figure 1.6. The main lens is in a 2f configuration, therefore $z_1 = z_2 = z$. The main lens forms an image of the object at the main lens plane, showed with a dashed line in figure 1.6 and the micro array system acts as a relay between the main lens image and the sensor forming the array of sub images as described in the previous sections.

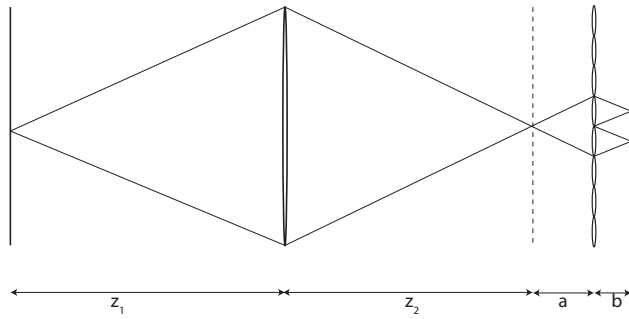


Figure 1.6: Ray diagram of the system simulated.

The main objective of running simulation on a plenoptic 2.0 system was to investigate its behaviour at diffraction limit as well as to better understand the trade-offs in resolution and how the different parameters of the systems effects it. Different combinations of the optical parameters of the system,

including main lens aperture, micro array pitch and magnification, have been tested. The modularity of the Fresnel simulation toolbox allows to easily change the simulations parameters independently and collect results. Once defined the dimension and the number of pixel on the sensor, the pitch and focal length of the lens let array, the focal length of the main lens and the magnification m of the micro array stage, the simulation toolbox is capable to set autonomously all the other simulation parameters in order to respect the f-number matching between the main lens and the lens let array. In a plenoptic 2.0 imaging system the f-number is matched when:

$$\frac{z_2}{d} = \frac{b}{p} \quad (1.11)$$

where referring to figure 1.6, d is the aperture of the main lens, p is the micro array pitch, and z_2 and b are respectively the distance from the main lens to the image plane and the distance from the micro lens array to the sensor. If the lens let array has a focal length equal to f_μ and a pitch equal to p , the value of the distance from the sensor b can be obtained by the magnification m as:

$$b = m f_\mu \left(1 + \frac{1}{m} \right) \quad (1.12)$$

Equation 1.12 has been obtained substituting the expression of the magnification $m = b/a$ into the lens equation $1/a + 1/b = 1/f_\mu$. Values of the parameter b as a function of the magnification can be seen plotted in figure 1.7

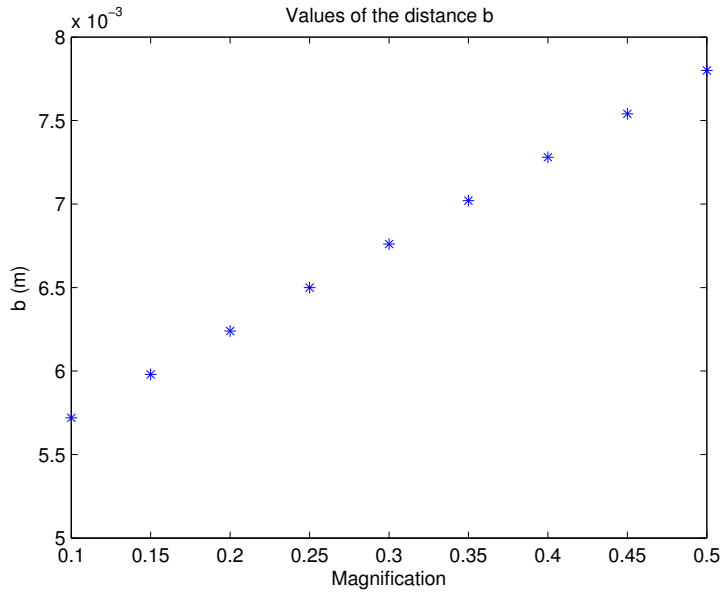


Figure 1.7: Values of the parameter b correspondent to values of magnification varying from 0.1 to 0.5.

Once b is defined the distance of the micro lens array from the main lens image is defined solving the lens law for a :

$$a = \frac{bf}{b-f} \quad (1.13)$$

Values of a as a function of the magnification can be seen in figure 1.8:

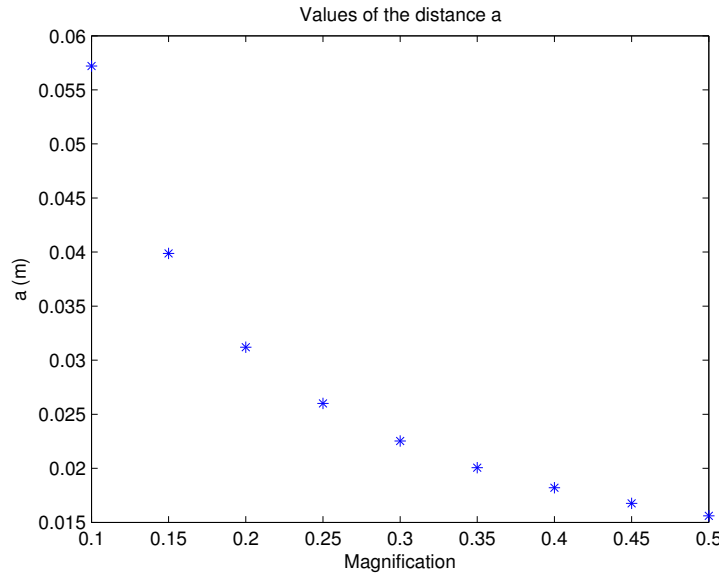


Figure 1.8: Values of the parameter b correspondent to values of magnification varying from 0.1 to 0.5.

Now that the relay system has been defined, the software defines the aperture of the main lens matching its f-number to the one of the lens let using equation 1.11. We have:

$$r_{lens} = \frac{zp}{2b} \quad (1.14)$$

Values of a as a function of the magnification can be seen in figure

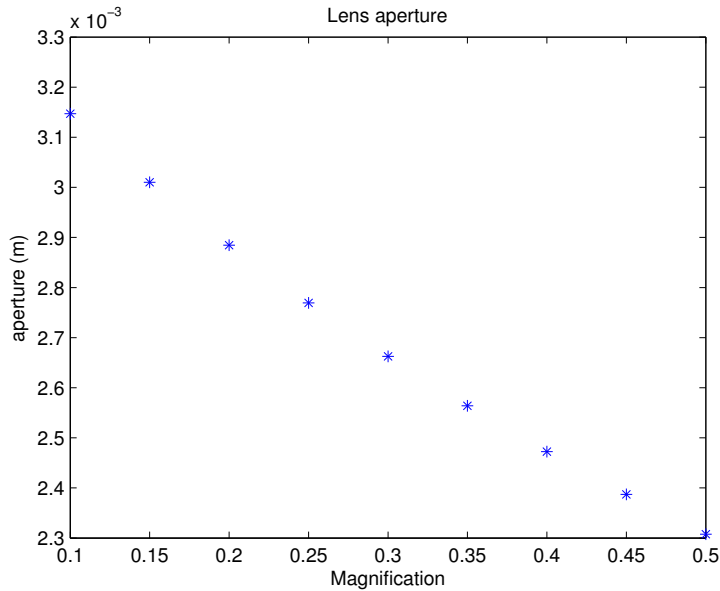


Figure 1.9: Aperture of the main lens as a function of the magnification in order to respect the f-number matching condition.

Therefore the simulation platform is able to set the simulations parameters when some other are given, making the launching procedure of each simulation easy and quick. We set the micro lens array with the following characteristic:

Array size	5.8 x 5.8 mm
Micro lens focal length f_μ	5.3 mm
Micro array pitch p	150 μm
sensor size	5.8 x 5.8 mm
sensor resolution	3500 by 3500 pixel
pixel size	1.67 μm
number of lens let	39 x 39 lens lets
main lens focal length	60 mm

And the values obtained for a, b and the main lens aperture corresponding to the magnification investigated are:

Magnification	<i>a</i>	<i>b</i>	main lens aperture
0.5	15.6 mm	7.8 mm	2.3 mm
0.3	22.5 mm	6.8 mm	2.7 mm
0.25	26 mm	6.5 mm	2.8 mm

1.3 Optical performances of a focused plenoptic system

In this section it will be shown the results obtained running simulations of the system described in section 1.2 at its diffraction limit. Three different configuration of the micro lens array stage has been tested, corresponding to the parameters a and b setted in order to have magnification $m = b/a$ equals to 0.5, 0.3 and 0.25. The first simulation presented is the image of a single focused point source. A comparison between the main lens image and the rendered image will be done to understand the differences in optical resolution and to evaluate the noise induced by the rendering algorithm. The optical resolution of an imaging system is defined by its impulse response, known as point spread function [16, 24]. If the input is a point source in focus, the output image has a well known intensity profile, the Airy disk. The Airy disk defines the broadening that a point source undergo after being imaged by an optical system, hence it is a good estimation of the minimum feature resolvable by the system [16, 35]. The Airy disk is shown in figure 1.10. The position of the first zero of the Airy disk is given by:

$$x_1 = 1.22\lambda F_\# \quad (1.15)$$

and the total extension of the central lobe is defined as the distance between the first two zeros as:

$$\Delta x = 2.44\lambda F_{\#} = 2.44\lambda \frac{b}{p} \quad (1.16)$$

where λ is the wavelength of the radiation, b is the distance between the lens let and the sensor and p is the pitch of the micro array and the aperture of the single lens let. In the central lobe is contained the 90% of the total energy of the optical field, therefore its extension defines the spread that each point undergoes in the final image.

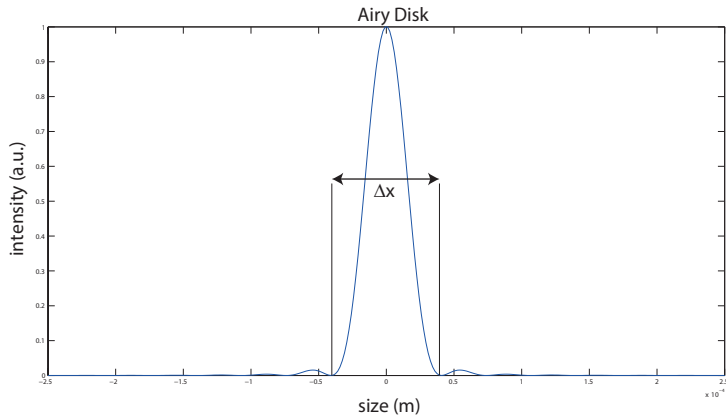


Figure 1.10: Aperture of the main lens as a function of the magnification in order to respect the f-number matching condition.

We define Δx is the optical resolution of the imaging system. In a plenoptic 2.0 system there are two elements that influences the optical resolution, the main lens and the micro lens array. Because of the f-number matching condition, the optical resolution in the two imaging stages should be the same. But because of the magnification present in the micro array stage, different than the magnification of the main lens, the coordinates in the main lens image plane are rescaled of a factor equal to the magnification m when imaged

by the micro array on the sensor [16]. If we use the coordinates x' and y' are the coordinates of the main lens image plane, the sub image coordinates will be given by:

$$\begin{cases} x = \frac{x'}{m} \\ y = \frac{y'}{m} \end{cases} \quad (1.17)$$

Therefore if a pixel on the main lens image samples a feature size of δx , on the sensor the same pixel will sample a quantity $\delta x/m$. Because m is smaller than 1, the spread of a point on the sensor plane will be bigger than the one on the main lens image plane. The same pixel samples a bigger area of the object in the image. This leads to a loss in optical resolution [36]. The smaller is the magnification, the broader becomes the point spread function and as a consequence the band pass of the micro lens array becomes narrower.

The optical cut off frequency is defined as:

$$\nu_{cutoff} = m \frac{1}{\lambda f_\#} = m \frac{b}{\lambda p} \quad (1.18)$$

In figure 1.11 are plotted the values of the lateral resolution in function of the magnification of the micro array stage, while in figure 1.12 are plotted the correspondent values of the optical cut off frequency.

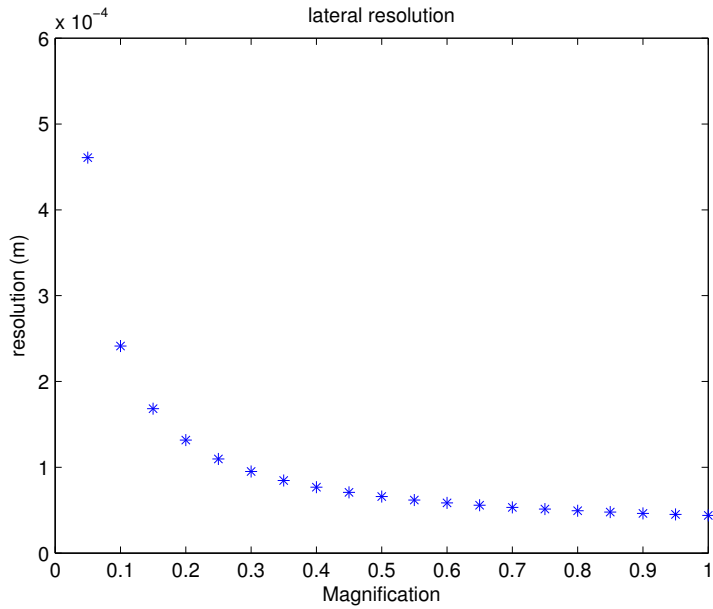


Figure 1.11: lateral resolution as a function of the magnification.

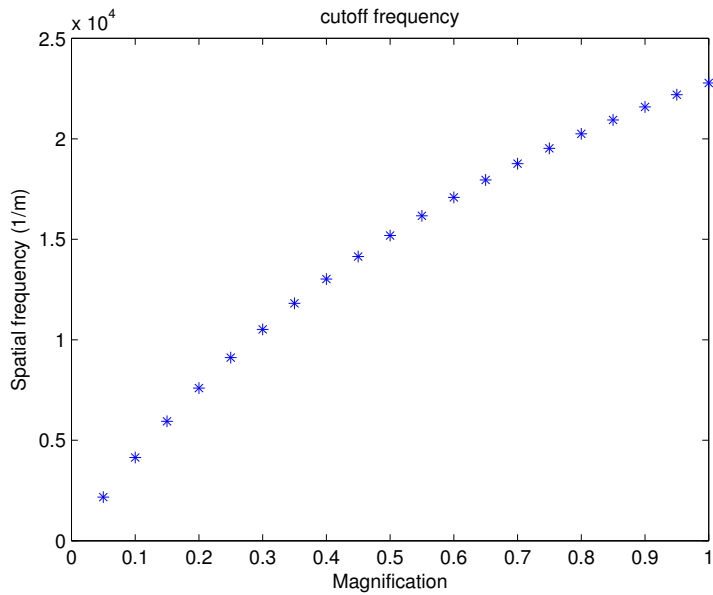


Figure 1.12: optical cut-off frequency as a function of the magnification.

This means that in a plenoptic 2.0 imaging system exists an intrinsic trade-off between optical resolution and spatio-angular resolution. The trade

off between spatial and angular resolution has been described in section ??.

A further trade off is now present and is it due to diffraction. A low magnification allows to sample very well the direction and therefore to have a finer axial resolution when evaluating depth but a magnification too low will filter out high frequency components of the object. In the next sections we will investigate in detail the optical performances of a focused plenoptic system, performing simulations to better understand the trade off between spatio-angular resolution and optical resolution.

1.4 Impulse response of a Focused Plenoptic system

The first simulation we perform will be focused to obtain the impulse response of a focused plenoptic system, that as we seen in section 1.3 is the Airy disk. To obtain the diffraction pattern generated by a point source we simulated such a source with a pupil with a diameter of $10 \mu m$. As explained in section 1.1, the magnification gives the number of point of views that a single point in the main lens image is imaged on the sensor plane. To have directional information, a point must be imaged at least by two lens lets per direction. In this way two set of directional coordinates are captured and on the sensor we expect to see each point repeated four times, two times horizontally and two vertically. With a magnification of 0.5, the sub images will be 2 per direction, with a magnification of 0.3 each point is expected to be replicated 3 times, and with a magnification of 0.25 four times. In figure , , and figure are shown the raw sensor images and the rendered images of a point source when the magnification is 0.5, 0.3 and 0.25.

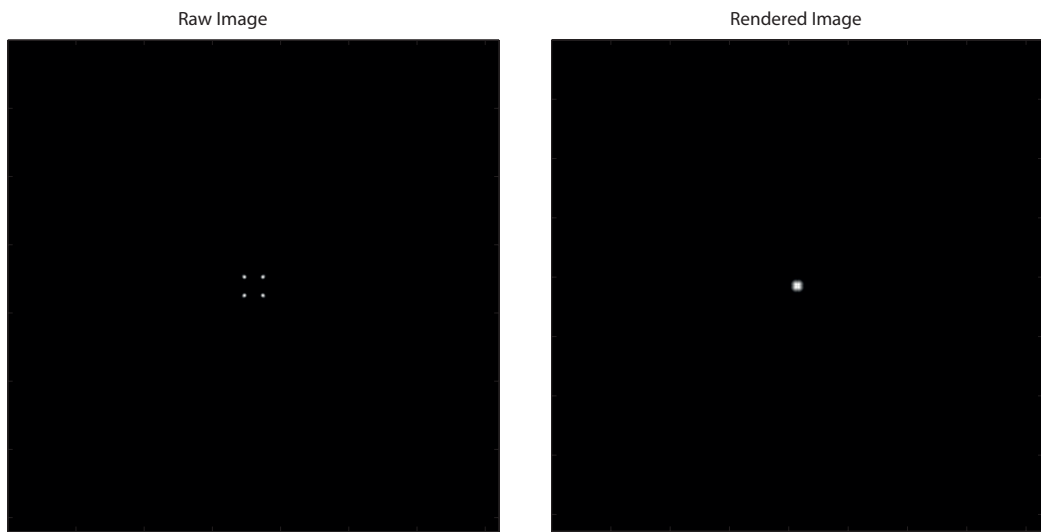


Figure 1.13: Left: raw sensor image, Right: rendered image. Artifacts are present. Magnification: 0.5

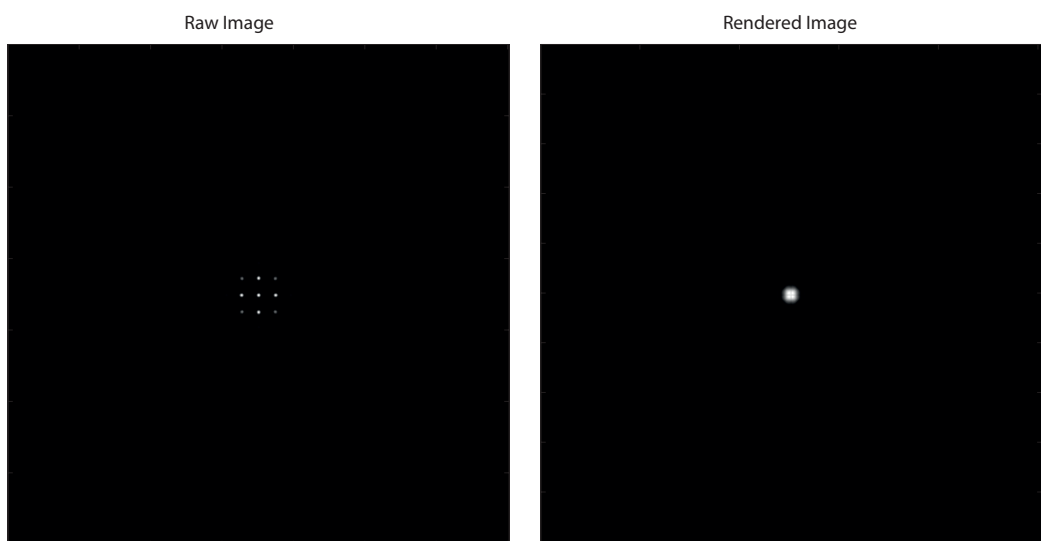


Figure 1.14: Left: raw sensor image, Right: rendered image. Artifacts are present. Magnification: 0.3.

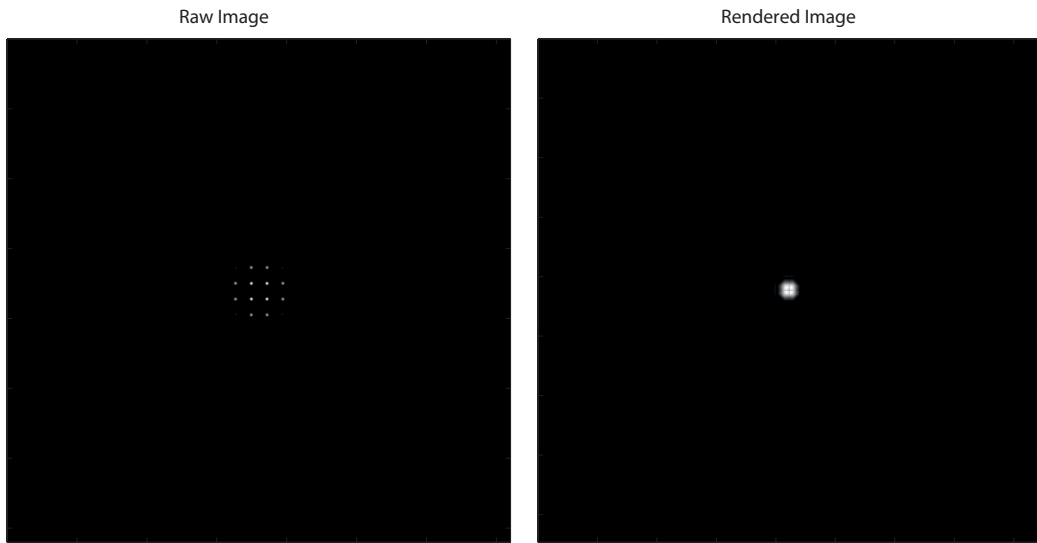


Figure 1.15: Left: raw sensor image, Right: rendered image. Artefacts are present. Magnification: 0.25

In figure 1.16 are shown the intensity profiles of the main lens image and of the rendered images. The profiles are obtained by sum all the rows of the matrix of the image and normalizing by its. It is clear in all three cases the difference in size of the central lobe of the impulse response.

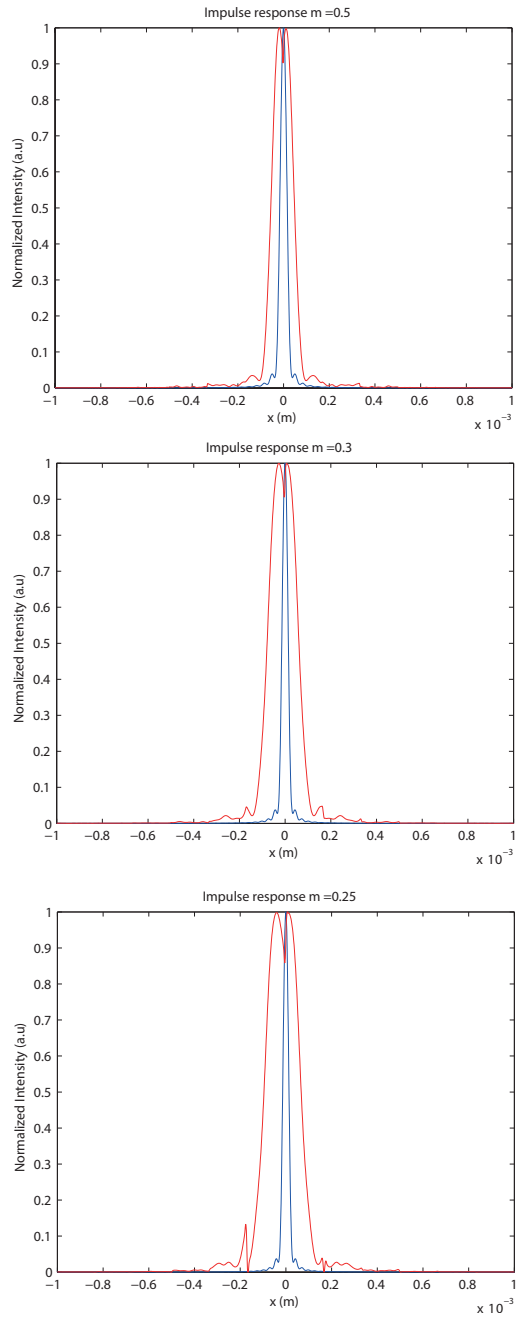


Figure 1.16: From top to bottom: comparison between the main lens image profile, in blue, and the rendered image profile, in red, for magnification values of 0.5, 0.3 and 0.25. The central lobe of the rendered image increase with the magnification, as well as the number of artefacts.

From figure 1.16 it is possible to appreciate the broadening effects of the central lobe of the rendered image intensity profile, in red, respect the main lens image. The central lobe size is also dependent by the magnification used as seen in figure 1.11. With a smaller magnification, the number of sub images that sample a single point source increase, and due to the nature of the rendering process explained in section 1.1.2, the number of artefacts increases, broadening even more the central lobe and making the lateral resolution worst. In table 1.4 are shown the values of the central lobe size of the main lens image, Δx , of the rendered image $\Delta x'$ and the ratio between them. Error in the ratio is due to the presence of artefacts generated by the rendering algorithm that increases with the decrease of the magnification.

Magnification	Δx (m)	$\Delta x'$ (m)	$\Delta x/\Delta x'$
0.5	7.848×10^{-5}	2×10^{-4}	0.392
0.3	6.848×10^{-5}	2.698×10^{-4}	0.25
0.25	6.514×10^{-5}	3.574×10^{-4}	0.18

1.5 Two point resolution

Another important instrument too evaluate the resolution of an imaging system is the Rayleigh criterion of resolution. It states that two incoherent point sources are resolved by a diffraction limited imaging system when the centre of the Airy disk intensity pattern generated by one point source falls exactly on the first zero of the Airy disk generated by the other point source [16]. Since a point source image is almost coherent, the two point sources should be out have different initial phases. Therefore the minimum distance

between two point sources whose relative phase differs for $\pi/2$ is:

$$\delta x = 1.22\lambda \frac{z}{d} \quad (1.19)$$

Where d is the lens aperture and z is the propagation distance. We simulated two point sources with at distance equal to the 1.19 and we evaluated the effect of the magnification of the micro array stage for a $m = 0.5$. Figure 1.17 represents the main lens image and the rendered image with their respective intensity profiles, of two point source with a diameter of $10 \mu m$ separated by a distance $\delta x = 40 \mu m$. the imaging system simulated is the same described in section 1.2.

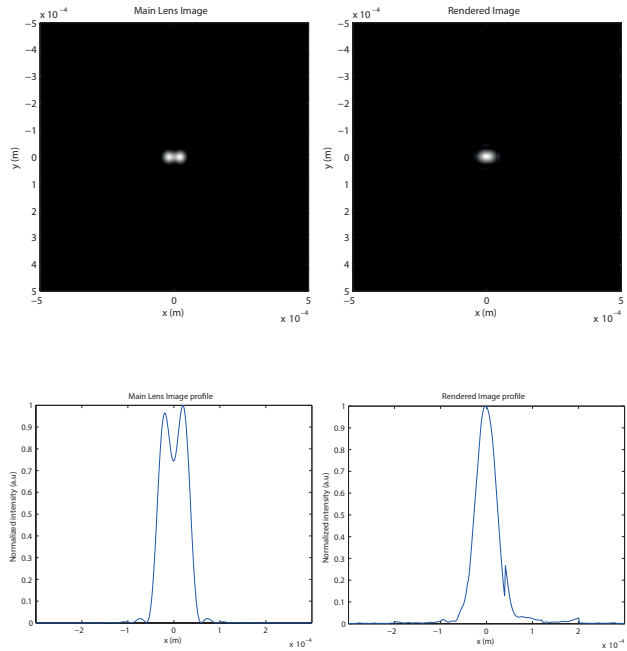


Figure 1.17: On the top left it is shown the main lens image of two point sources separated by the Rayleigh distance δx . On the top right its corresponded rendered plenoptic image obtained with a magnification of 0.5. As expected from the theory, the resolution of the rendered image is half the one af the main lens image, and the two points are no more distinguishable as confirmed by the intensity profiles of the two images on the bottom.

While in the main lens image we are at the limit of resolution and the two points are still resolvable, in the rendered image the two spot sizes are merged together and resolve the two point sources in no more possible. Since the magnification of the plenoptic imaging system is $m = 0.5$, its optical resolution in the rendered image will be half of the resolution of the main lens, as shown in section 1.3. Therefore if we double the separation between the point sources we should be able to resolve them also in the rendered image. In figure 1.18 we have the simulations results for a $\delta x = 80\mu m$:

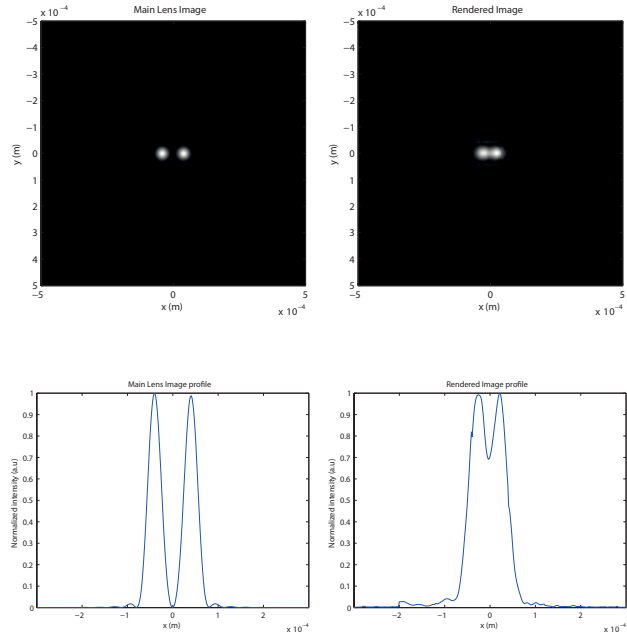


Figure 1.18: In the top left it is shown the main lens image of two point sources separated by the Rayleigh distance $2\delta x$. On the top right its corresponded rendered plenoptic image obtained with a magnification of 0.5. Doubling the Rayleigh distance we obtained a rendered image at the limit of resolution, where the maximum of the Airy pattern of one point falls on the first zero of the second point.

This results obtained simulating wave optics propagation in the plenoptic imaging system confirm the predictions made in section 1.3. When imaging

an object with a plenoptic 2.0 system the loss of resolution due to the magnification should be taken into account in order not to lose useful information in the sample, or a suitable lens let array configuraqtion should be chosen.

1.6 Frequency analysis of a focused plenoptic system

We now analyse the frequency response of a focused plenoptic system. The Spatial frequencies that are transferred from the object to the image plane in an optical system are defined by its modulation transfer function (MTF). The MTF is defined as the square modulus of the Fourier transform of the impulse response $h(x,y)$ of an optical system [16].

It is then:

$$H(f_x, f_y) = |\mathcal{F}\{h(x, y)\}| \quad (1.20)$$

It represents the weighting factor applied by the system to all the frequency components of the optical field coming form the object. The visibility and the contrast of the points corresponding to the different values of spacial frequency changes according to the modulation imposed by the MTF. When it goes to zero, no energy is transmitted for that particular frequency and the detail becomes invisible. The value of spatial frequency for which the MTF goes to zero is called optical cut-off frequency. In this section we investigate the effects of the magnification on the location of optical cut-off frequency. The first result presented is the obtained calculating the modulation transfer function of the plenoptic 2.0 system described in section 1.4, with a magnification values of 0.5, 0.3 and 0.25. The MTF of these three cases are shown in

1.6. FREQUENCY ANALYSIS OF A FOCUSED PLENOPTIC SYSTEM29

figure 1.19, 1.20 and 1.21 and have been obtained applying equation 1.20 to the intensity profiles in figure 1.16. In all the three figures, in green is shown MTF of the single lens imaging system, without the lens let array stage, and in red the MTF of the plenoptic system.

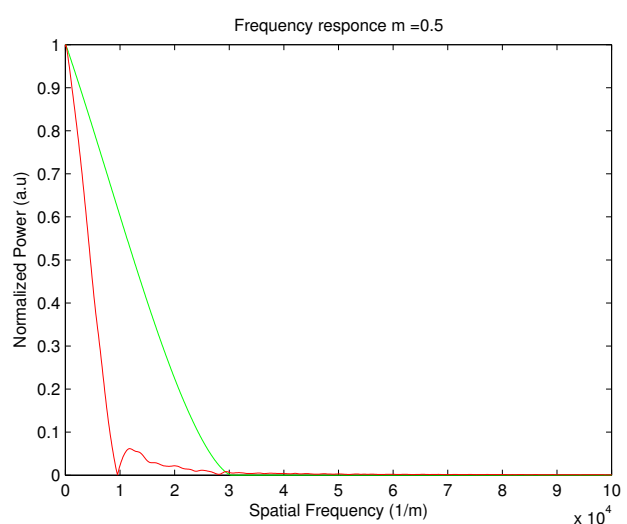


Figure 1.19: Modulation transfer functions of the main lens (green) and the overall imaging system (red) for a magnification value of $m = 0.5$

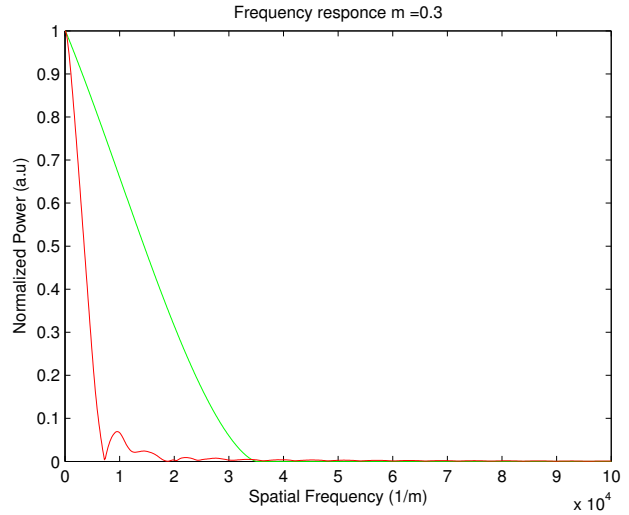


Figure 1.20: Modulation transfer functions of the main lens (green) and the overall imaging system (red) for a magnification value of $m = 0.3$

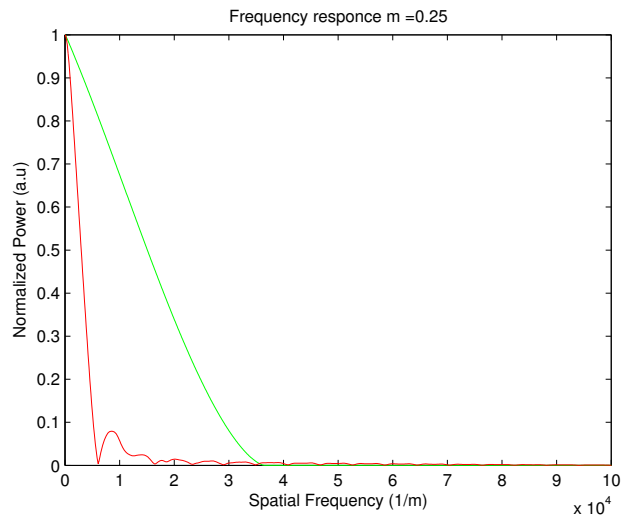


Figure 1.21: Modulation transfer functions of the main lens (green) and the overall imaging system (red) for a magnification value of $m = 0.25$

From figure 1.19, 1.20 and 1.21 we can see that the cut off frequency of the single lens system increases with the decreasing of the magnification, while the cut-off frequency decrease with the decreasing of the magnification

if the lens let array stage is added. This result is in accord with what seen in sections 1.3 and is a direct consequence of the simulations results shown in section 1.4. The values of the cut-off frequencies obtained by the simulations are:

Magnification	Rendered $f_{cut-off}$ (1/m)	Main lens $f_{cut-off}$ (1/m)
0.5	1×10^4	3×10^4
0.3	0.756×10^4	3.5×10^4
0.25	0.63×10^4	3.6×10^4

The second set of simulations done evaluates the effects of the magnification in more detail. A varying frequency sinusoidal grating is imaged incoherently, as explained in chapter ??, by the system with the same three different configurations of the micro array stage. The Grating contains five different frequencies :

$$\begin{array}{l|l} f_1 & 0.1 \times 10^4 \text{1/m} \\ f_2 & 0.8 \times 10^4 \text{1/m} \\ f_3 & 1.518 \times 10^4 \text{1/m} \\ f_4 & 2.22 \times 10^4 \text{1/m} \\ f_5 & 2.936 \times 10^4 \text{1/m} \end{array}$$

This sinusoidal pattern is shown in figure 1.22 has been imaged with the same three different configurations of the lens let array in order to have a magnification of: $m = 0.5$, $m = 0.3$ and $m = 0.25$.

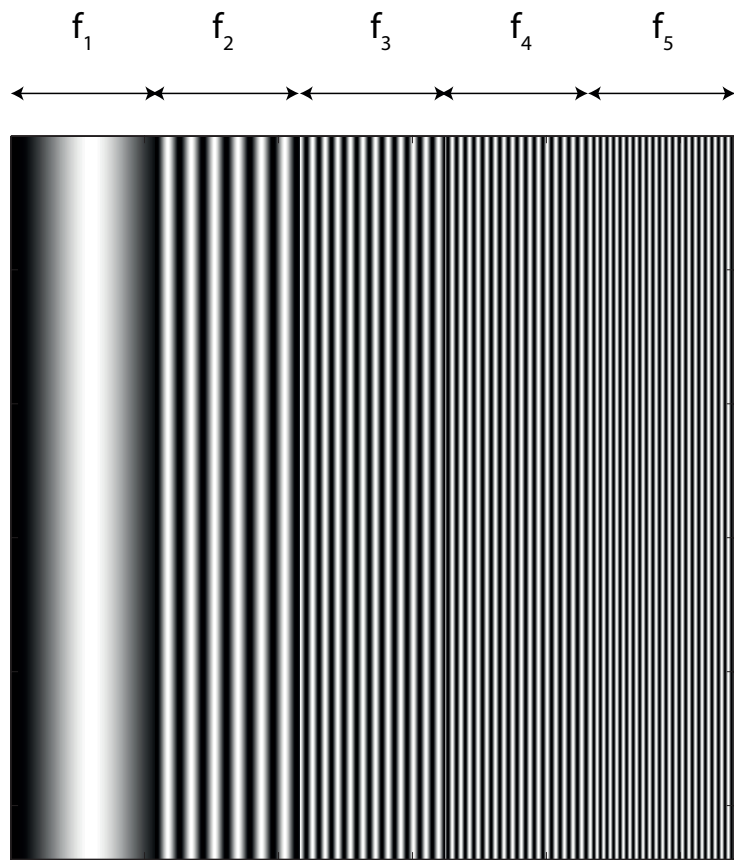


Figure 1.22: The object imaged in this simulation is a sinusoidal grating containing five different frequencies.

In figure 1.23 are shown the raw image, the main lens image and rendered images of the sinusoidal grating shown in figure 1.22, imaged with a magnification of $m = 0.5$. The two rendered images are obtained with the basic rendering explained in section 1.1. To remove digital artefacts given by the tiling of the sub images patches on the rendered images a low pass Gaussian filter with $\sigma = 1.162 \times 10^4$ has been applied.

1.6. FREQUENCY ANALYSIS OF A FOCUSED PLENOPTIC SYSTEM 33

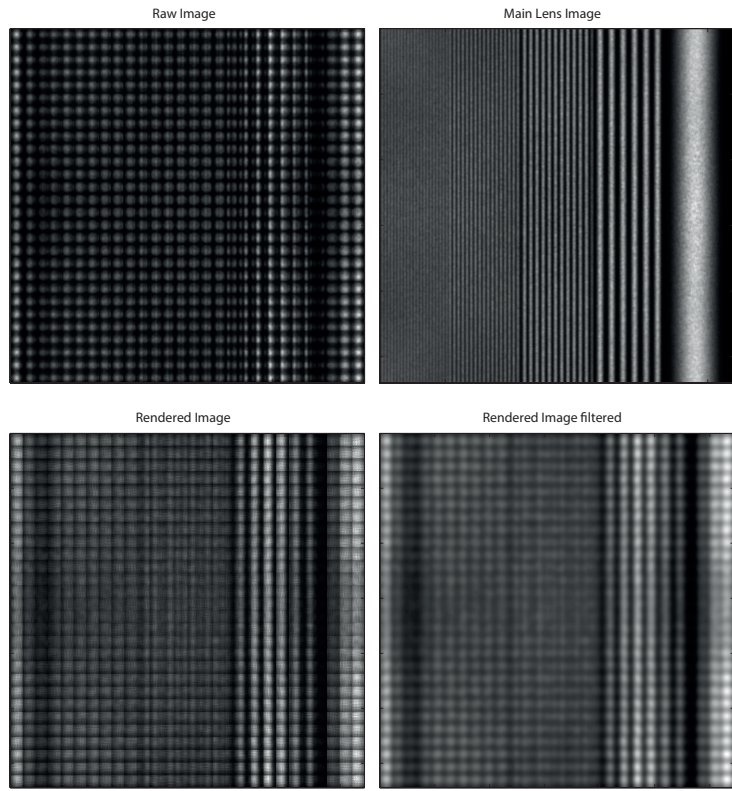


Figure 1.23: Top: on the left it is shown the raw sensor image, on the right the main lens image. Bottom: On the left there is the rendered image, on the right the same image has been low pass filtered to remove some of the rendering artefacts. Magnification was 0.5

The normalized intensity profile of the optical field at the main lens image plane compared with the intensity profile of the rendered image is shown in figure 1.24 on the left side. On the right are shown the power spectra of the main lens image and of the rendered image. The modulation transfer function of the main lens and of the full plenoptic system has been added in red.

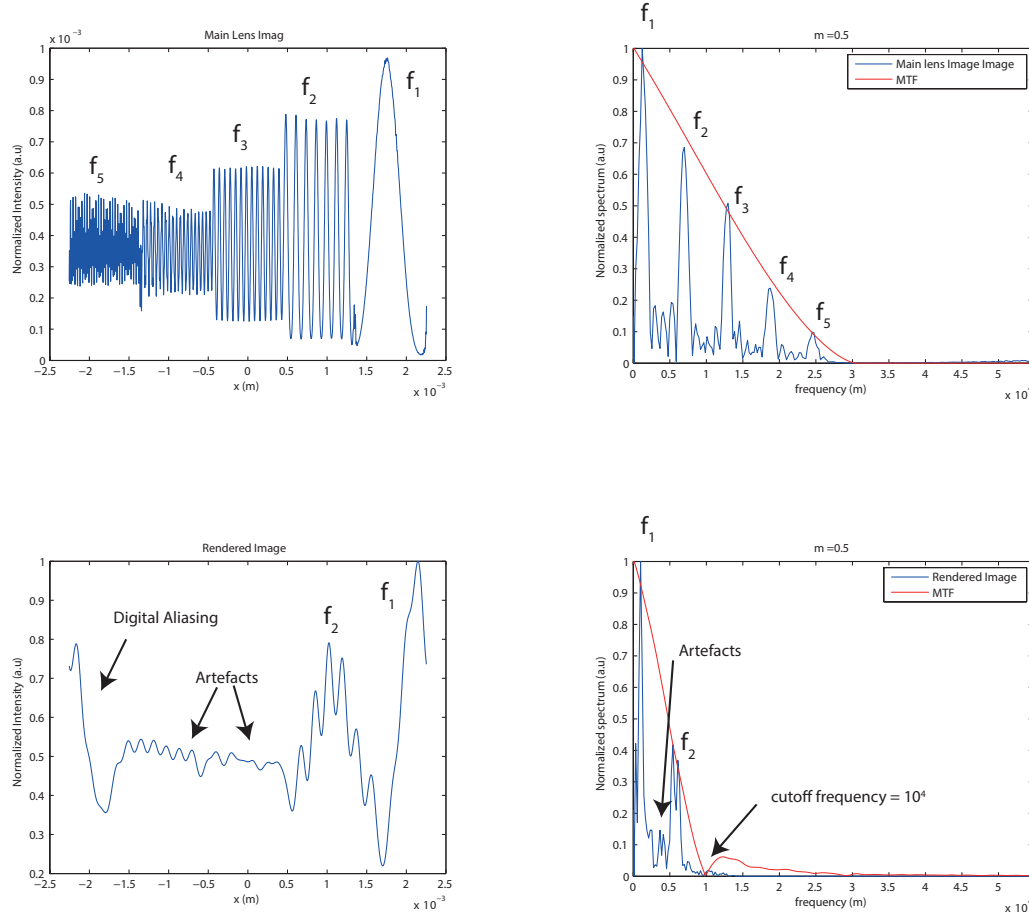


Figure 1.24: On the left are plotted the intensity profiles of the main lens image, top and of the rendered image, bottom. Spatial frequencies are modulated according to the MTF as shown by the power spectra of the main lens image on the top right and of the rendered image on the bottom right. The magnification of the lens let array is $m = 0.5$ and cut-off frequency of the system is $f_{cut-off} = 10^4 \text{ m}$

As expected the amplitude of the oscillations in both the main lens image and the rendered image follow the profile of the modulation transfer function of the two stages. Not all the frequency components of the object field are transmitted through the different stages of the plenoptic imaging system. In

1.6. FREQUENCY ANALYSIS OF A FOCUSED PLENOPTIC SYSTEM35

fact it acts ad a low pass filter, whose bandwidth depends on the magnification used in the lens let array stage. The low pass filtering action is shown in figure 1.25.

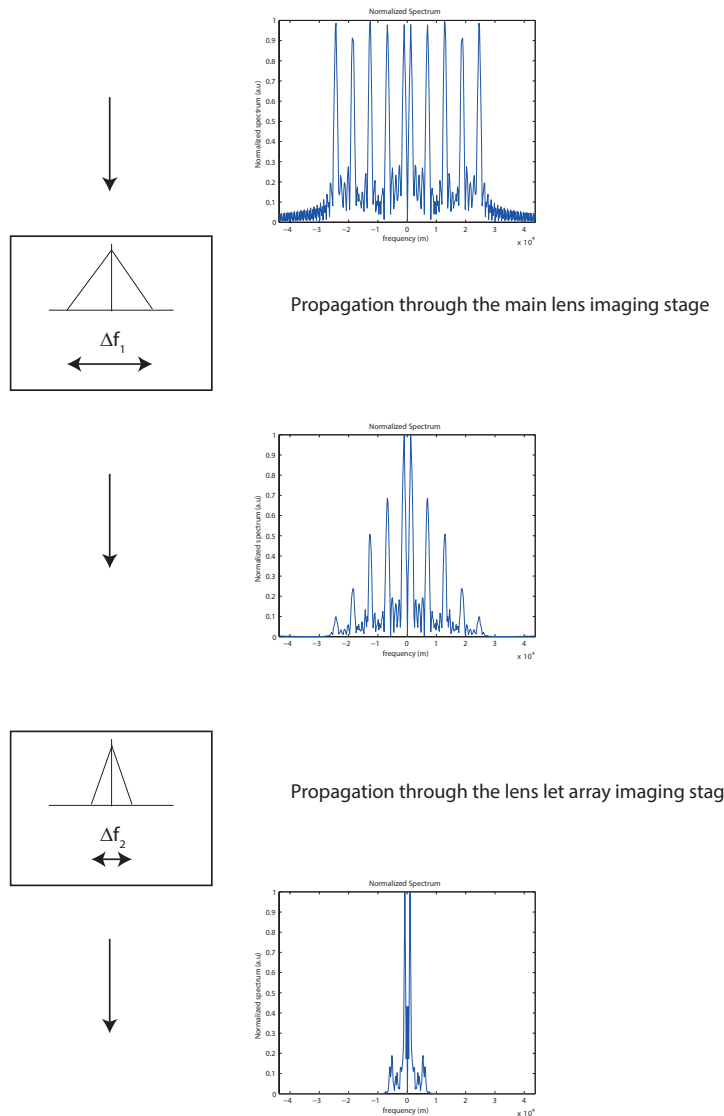


Figure 1.25: Evolution of the spectrum of the optical field as it propagates through the imaging system. The imaging system is modelled as a linear low pass filter with a bandwidth δf_2 defined by the magnification of the micro array stage.

It is interesting to see also that in the rendered image presents some artefacts which are responsible for some extra frequencies present in the spectrum of the output rendered image. The cut off frequency of the imaging system with a magnification equal to 0.5, is $10^4 1/m$, therefore only the first two frequencies will be transmitted to the rendered image, as shown in figure 1.24. If the magnification drops to $m = 0.3$ the bandwidth of the system gets narrower, and more frequencies are not transmitted in the rendered image. In figure 1.26 are shown the raw image, the main lens image and rendered images of the sinusoidal grating shown in figure 1.22

1.6. FREQUENCY ANALYSIS OF A FOCUSED PLENOPTIC SYSTEM37

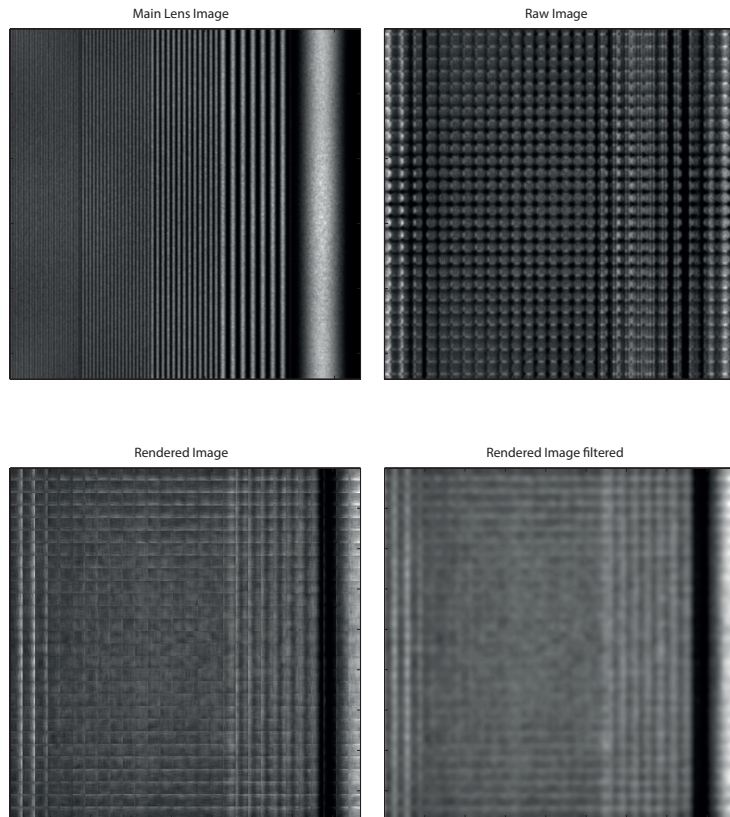


Figure 1.26: Top: on the left it is shown the raw sensor image, on the right the main lens image. Bottom: On the left there is the rendered image, on the right the same image has been low pass filtered to remove some of the rendering artefacts. Magnification was 0.3.

And as we did for the previous case, we compare the intensity profile s of the main lens image with the rendered image their power spectra in figure 1.27.

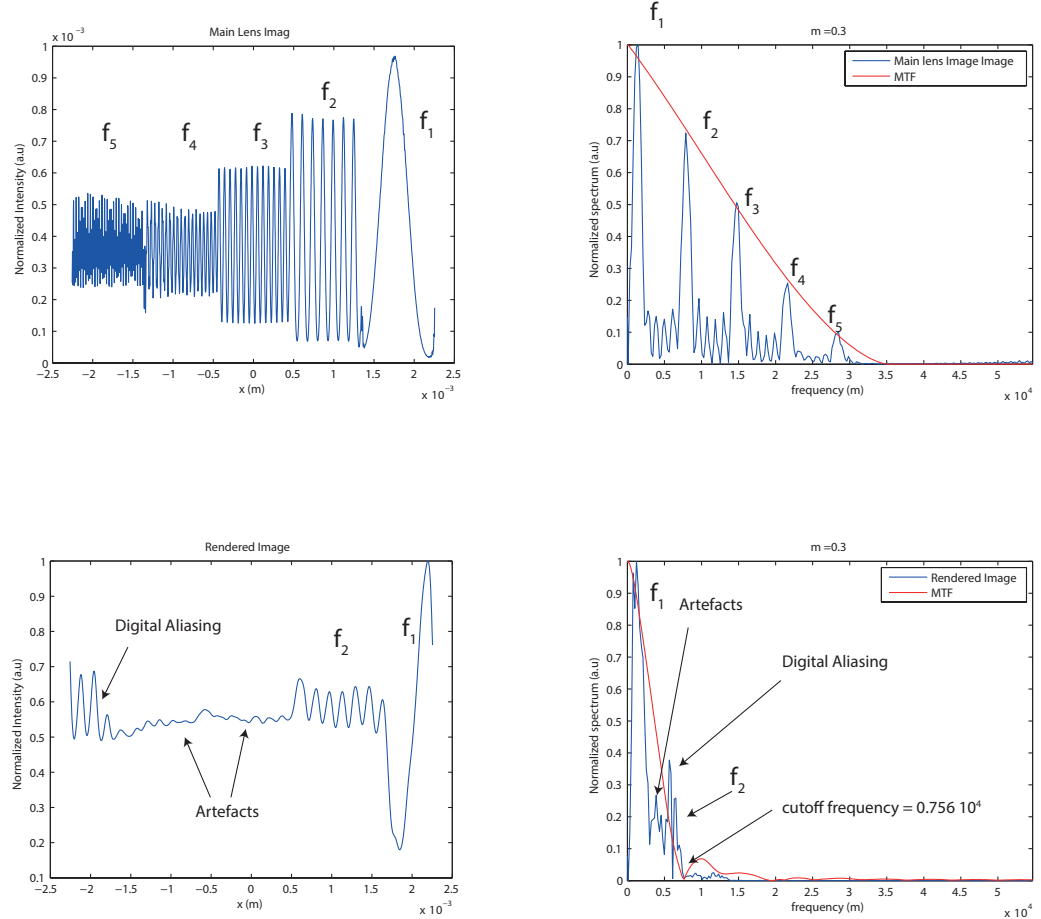


Figure 1.27: On the left are plotted the intensity profiles of the main lens image, top and of the rendered image, bottom. Spatial frequencies are modulated according to the MTF as shown by the power spectra of the main lens image on the top right and of the rendered image on the bottom right. The cut-off frequency of the system is $0.756 \times 10^4 \text{ m}$

From figure 1.27 we can see that the frequency f_2 gets dimmed more respect the previous case because it is closer to the cut-off frequency of the system. The spectrum of the rendered image allows to discriminate between frequencies due to artefacts in the rendering process since their power is less than the expected value predicted by the modulation transfer function for

that frequency. These frequencies are indicated in figure 1.27 with an arrow as artefacts. In profile it is very clear some digital aliasing. Low frequencies components generated due to aliasing have been picked up by the relay stage and transmitted to the rendered image. This frequencies are indicated in figure 1.27 as "Digital Aliasing". This effects can be seen in detail in figure 1.28:

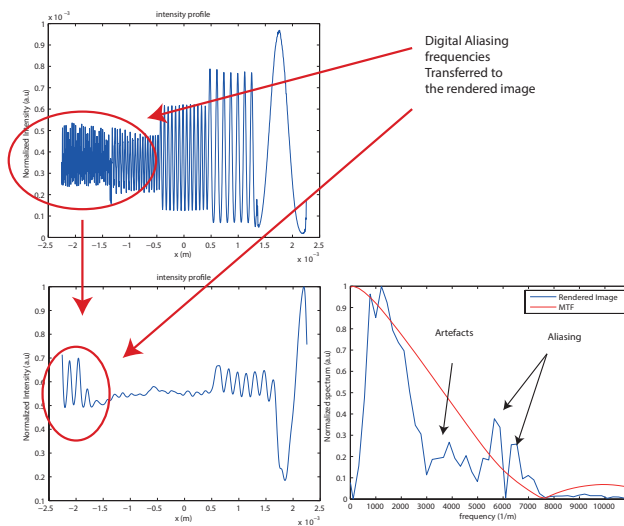


Figure 1.28: Aliased frequencies transmitted to the rendered image.

This happens because the low frequencies of the envelope of the oscillations in the far left side of the main lens image fall under the micro array modulation transfer function and are therefore transmitted modulated to the rendered image.

If the magnification is 0.25 we have the situation shown in figure 1.29 and figure 1.30.

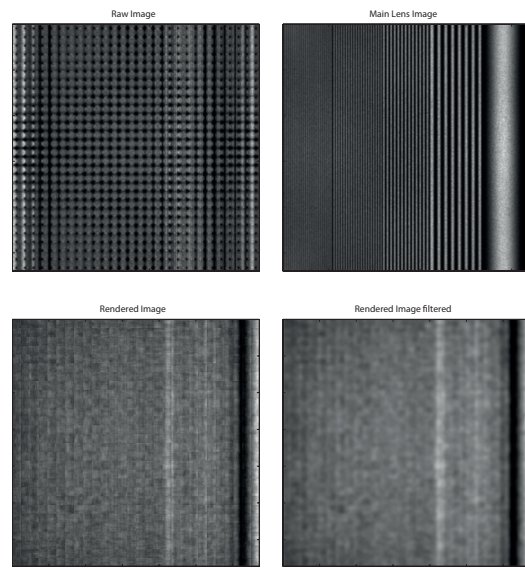


Figure 1.29: Top: on the left it is shown the raw sensor image, on the right the main lens image. Bottom: On the left there is the rendered image, on the right the same image has been low pass filtered to remove some of the rendering artefacts. Magnification was 0.3.

1.6. FREQUENCY ANALYSIS OF A FOCUSED PLENOPTIC SYSTEM 41

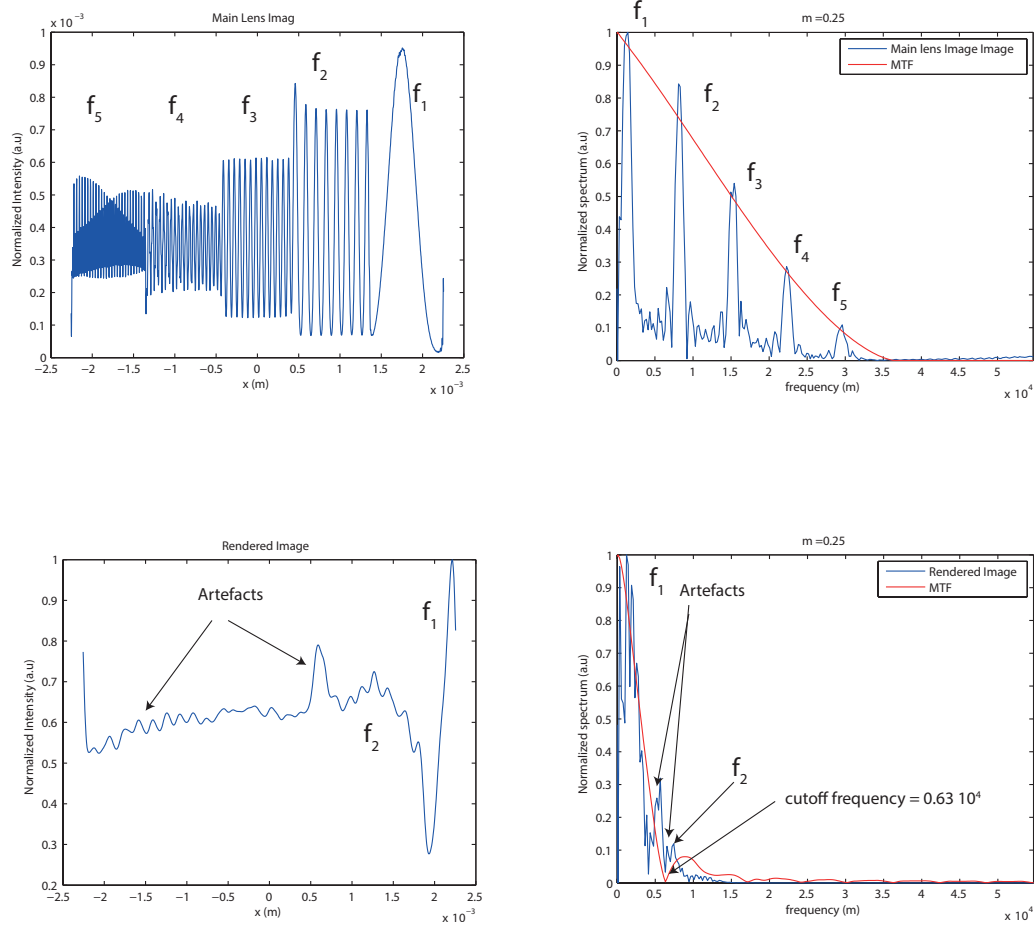


Figure 1.30: On the left are plotted the intensity profiles of the main lens image, top and of the rendered image, bottom. Spatial frequencies are modulated according to the MTF as shown by the power spectra of the main lens image on the top right and of the rendered image on the bottom right. The cut-off frequency of the system is $0.6 \times 10^4 \text{ m}^{-1}$

In figure 1.30 we see that with a lower magnification, the digital aliasing frequencies are no more transmitted to the rendered image. This is due to the fact that with a narrower bandwidth of the modulation transfer function these frequencies are filtered out of the signal. The same happens to the

frequency f_2 of the object field, since the cut off frequency for a magnification equal to 0.25 is lower than the signal frequency f_2 .

1.7 Conclusions

In this chapter has been carried on a frequency analysis of a focused plenoptic system, in order to investigate its behaviour at its diffraction limit. We analysed the optical performances of the plenoptic imaging system treating it as a linear system with a finite bandwidth that depends by the magnification of the lens let array. The distances a and b not only define the angular resolution of the system and the trade off with spatial resolution, but also allows to quantify the limits of the system in terms of optical resolution. This is a new contribution to the field, since it has been formalized what was first presented in 2014 by Turola *et al.* [36]. To know how optical frequencies are transmitted through the system allows to design its components in order to satisfy the requirements imposed by the practical application encountered. The optical resolution degradation with the increase of the angular resolution represents an intrinsic limitation to plenoptic 2.0 imaging system especially in applications regarding microscopy, where diffraction limit is very important. To overtake this limitations we can do two things. The first approach consists in improving the basic optical elements of the system, that is choosing low f-number optical elements, larger array of micro lenses and sensors, or improving the optics before the micro array stage in order to deliver pre processed optical frequencies that wont be affected by the loss of resolution in the relay stage. It is also possible to act on the micro lens array, creating an array of lens lets with different focal length [37]. This approach

could results in expensive devices, and it is preferable to approach this issue computationally. Raw plenoptic data can be elaborated in post processing and can lead to a full sensor resolution rendering, and even a super resolution rendering as done by Georgiev *et al.* [26, 28, 38, 30, 39], by Favaro an Bishop *et al.* [40, 41, 42, 29] and Shroff *et al.* [43, 44]. Another way to overcome the loss of resolution is to design an hybrid system composed by two branches, o plenoptic branch and and a conventional high resolution branch. This hybrid systems [45, 46], are based on the simultaneously acquisition of a plenoptic and a high resolution image that will be used a base to interpolate the plenoptic data in order to fill the gaps in resolution. In the next chapter we will apply the knowledge and the experience acquired designing and testing simulated plenoptic imaging system to design a real optical setup, and we will discuss the results obtained.

Bibliography

- [1] Shree K Nayar. Computational cameras: Redefining the image. *Computer*, (8):30–38, 2006.
- [2] Ren Ng. *Digital light field photography*. PhD thesis, stanford university, 2006.
- [3] Todor Georgiev and Andrew Lumsdaine. Focused plenoptic camera and rendering. *Journal of Electronic Imaging*, 19(2):021106–021106, 2010.
- [4] Levoy Mark. Stanford light field microscope project, 2005.
- [5] Changyin Zhou and Shree K Nayar. Computational cameras: Convergence of optics and processing. *Image Processing, IEEE Transactions on*, 20(12):3322–3340, 2011.
- [6] Edward H Adelson and James R Bergen. *The plenoptic function and the elements of early vision*. Vision and Modeling Group, Media Laboratory, Massachusetts Institute of Technology, 1991.
- [7] Edward H Adelson and John Y. A. Wang. Single lens stereo with a plenoptic camera. *IEEE Transactions on Pattern Analysis & Machine Intelligence*, (2):99–106, 1992.

- [8] Marc Levoy and Pat Hanrahan. Light field rendering. In *Proceedings of the 23rd annual conference on Computer graphics and interactive techniques*, pages 31–42. ACM, 1996.
- [9] Todor Georgiev and Chintan Intwala. Light field camera design for integral view photography. *Adobe System, Inc*, 2006.
- [10] Ren Ng, Marc Levoy, Mathieu Brédif, Gene Duval, Mark Horowitz, and Pat Hanrahan. Light field photography with a hand-held plenoptic camera. *Computer Science Technical Report CSTR*, 2(11), 2005.
- [11] Andrew Lumsdaine and Todor Georgiev. Full resolution lightfield rendering. *Indiana University and Adobe Systems, Tech. Rep*, 2008.
- [12] Andrew Lumsdaine and Todor Georgiev. The focused plenoptic camera. In *Computational Photography (ICCP), 2009 IEEE International Conference on*, pages 1–8. IEEE, 2009.
- [13] Victor Guillemin and Shlomo Sternberg. *Symplectic techniques in physics*. Cambridge University Press, 1990.
- [14] Todor Georgiev, Andrew Lumsdaine, and Sergio Goma. Plenoptic principal planes. In *Imaging Systems and Applications*, page JTuD3. Optical Society of America, 2011.
- [15] Arnold Sommerfeld. Optics lectures on theoretical physics, vol. iv. *Optics Lectures on Theoretical Physics, Vol. IV by Arnold Sommerfeld New York, NY: Academic Press INC, 1954*, 1, 1954.

- [16] Joseph W Goodman. *Introduction to Fourier optics*. Roberts and Company Publishers, 2005.
- [17] Maciej Sypek. Light propagation in the fresnel region. new numerical approach. *Optics communications*, 116(1):43–48, 1995.
- [18] Rafael C Gonzalez, Richard Eugene Woods, and Steven L Eddins. *Digital image processing using MATLAB*. Pearson Education India, 2004.
- [19] Kyoji Matsushima and Tomoyoshi Shimobaba. Band-limited angular spectrum method for numerical simulation of free-space propagation in far and near fields. *Optics express*, 17(22):19662–19673, 2009.
- [20] Maciej Sypek. Reply to the comment on “light propagation in the fresnel region–new numerical approach”. *Optics Communications*, 282(6):1074–1077, 2009.
- [21] Max Born and Emil Wolf. *Principles of optics: electromagnetic theory of propagation, interference and diffraction of light*. Cambridge university press, 1999.
- [22] Joseph W Goodman and Randy L Haupt. *Statistical optics*. John Wiley & Sons, 2015.
- [23] Emil Wolf. *Introduction to the Theory of Coherence and Polarization of Light*. Cambridge University Press, 2007.
- [24] Frank L Pedrotti and Leno S Pedrotti. Introduction to optics 2nd edition. *Introduction to Optics 2nd Edition by Frank L. Pedrotti, SJ, Leno S. Pedrotti New Jersey: Prentice Hall, 1993, 1, 1993*.

- [25] Todor G Georgiev and Andrew Lumsdaine. Resolution in plenoptic cameras. In *Computational Optical Sensing and Imaging*, page CTuB3. Optical Society of America, 2009.
- [26] Todor Georgiev and Andrew Lumsdaine. Superresolution with plenoptic camera 2.0. *Adobe Systems Incorporated, Tech. Rep*, 2009.
- [27] Gordon Wetzstein, Ivo Ihrke, Douglas Lanman, and Wolfgang Heidrich. Computational plenoptic imaging. In *Computer Graphics Forum*, volume 30, pages 2397–2426. Wiley Online Library, 2011.
- [28] Todor G Georgiev and Andrew Lumsdaine. Super-resolution with the focused plenoptic camera, November 20 2012. US Patent 8,315,476.
- [29] Tom E Bishop, Sara Zanetti, and Paolo Favaro. Light field superresolution. In *Computational Photography (ICCP), 2009 IEEE International Conference on*, pages 1–9. IEEE, 2009.
- [30] Todor Georgiev. Plenoptic camera resolution. In *Computational Optical Sensing and Imaging*, pages JTh4A–2. Optical Society of America, 2015.
- [31] Todor Georgiev, Ke Colin Zheng, Brian Curless, David Salesin, Shree Nayar, and Chintan Intwala. Spatio-angular resolution tradeoffs in integral photography. *Rendering Techniques*, 2006:263–272, 2006.
- [32] Christian Perwass and Lennart Wietzke. Single lens 3d-camera with extended depth-of-field. In *Proc. SPIE*, volume 8291, page 829108, 2012.
- [33] Michael Hansen and Eric Holk. Depth map estimation for plenoptic images. 2011.

- [34] Ole Johannsen, Christian Heinze, Bastian Goldluecke, and Christian Perwass. On the calibration of focused plenoptic cameras. In *Time-of-Flight and Depth Imaging. Sensors, Algorithms, and Applications*, pages 302–317. Springer, 2013.
- [35] Hans Peter Herzig. *Micro-optics: elements, systems and applications*. CRC Press, 1997.
- [36] Massimo Turola and Steve Gruppetta. Wave optics simulations of a focused plenoptic system. In *Frontiers in Optics*, pages JTU3A–24. Optical Society of America, 2014.
- [37] Todor Georgiev and Andrew Lumsdaine. The multifocus plenoptic camera. In *IS&T/SPIE Electronic Imaging*, pages 829908–829908. International Society for Optics and Photonics, 2012.
- [38] Todor Georgiev, Georgi Chunev, and Andrew Lumsdaine. Superresolution with the focused plenoptic camera. In *IS&T/SPIE Electronic Imaging*, pages 78730X–78730X. International Society for Optics and Photonics, 2011.
- [39] Todor G Georgiev, Andrew Lumsdaine, and Sergio Goma. High dynamic range image capture with plenoptic 2.0 camera. In *Signal recovery and synthesis*, page SWA7P. Optical Society of America, 2009.
- [40] Paolo Favaro. A split-sensor light field camera for extended depth of field and superresolution. In *SPIE Photonics Europe*, pages 843602–843602. International Society for Optics and Photonics, 2012.

- [41] Tom E Bishop and Paolo Favaro. The light field camera: Extended depth of field, aliasing, and superresolution. *Pattern Analysis and Machine Intelligence, IEEE Transactions on*, 34(5):972–986, 2012.
- [42] Tom E Bishop and Paolo Favaro. Full-resolution depth map estimation from an aliased plenoptic light field. In *Computer Vision–ACCV 2010*, pages 186–200. Springer, 2011.
- [43] Sapna Shroff and Kathrin Berkner. High resolution image reconstruction for plenoptic imaging systems using system response. In *Computational Optical Sensing and Imaging*, pages CM2B–2. Optical Society of America, 2012.
- [44] Sapna A Shroff and Kathrin Berkner. Image formation analysis and high resolution image reconstruction for plenoptic imaging systems. *Applied optics*, 52(10):D22–D31, 2013.
- [45] Chien-Hung Lu, Stefan Muenzel, and Jason Fleischer. High-resolution light-field microscopy. In *Computational Optical Sensing and Imaging*, pages CTh3B–2. Optical Society of America, 2013.
- [46] Vivek Boominathan, Kaushik Mitra, and Ashok Veeraraghavan. Improving resolution and depth-of-field of light field cameras using a hybrid imaging system. In *Computational Photography (ICCP), 2014 IEEE International Conference on*, pages 1–10. IEEE, 2014.